

$^{194,196,198}\text{Pt}(p, p')$ reactions at 35 MeVP. T. Deason,* C. H. King,[†] R. M. Ronningen, T. L. Khoo,[‡] F. M. Bernthal, and J. A. Nolen, Jr.*Departments of Chemistry and Physics and Cyclotron Laboratory, Michigan State University, East Lansing, Michigan 48824*

(Received 14 October 1980)

The $^{194,196,198}\text{Pt}(p, p')$ reactions have been studied at a proton energy of 35 MeV using nuclear emulsion plates and a high-resolution position-sensitive proportional counter. Approximately 45 levels were populated in each reaction. In ^{198}Pt , 38 of 44 levels to about 3.2 MeV are reported for the first time. Angular distributions from 20° to 110° were measured for many of these levels. Several new J^π assignments were made using empirical shapes of transitions to well-known levels in Pt. The results for the $J^\pi = 0^+, 2^+, 4^+$, and (for ^{194}Pt) 6^+ members of the ground band and the $2^+, 3^+$, and 4^+ members of the "quasi- γ " band were analyzed by coupled channels calculations incorporating relative transition strengths from the interacting boson approximation model. The multipole moments of the deformed optical model potential were calculated and compared to moments deduced from other studies.

NUCLEAR REACTIONS $^{194}\text{Pt}(p, p')$, $^{196}\text{Pt}(p, p')$, $^{198}\text{Pt}(p, p')$, $E_p = 35$ MeV; measured $\sigma(E_p, \theta)$; deduced energies, J^π ; coupled channels calculations, interacting boson approximation model; deduced optical model and deformation parameters, quadrupole and hexadecapole moments; comparisons to Coulomb excitation, (α, α') , and $(^{12}\text{C}, ^{12}\text{C}')$; enriched targets, nuclear emulsion plates (7 keV FWHM) and position-sensitive proportional counter (15 keV FWHM), magnetic spectrograph.

I. INTRODUCTION

The transitional region between the well-deformed rare-earth nuclei and the spherical nuclei near ^{208}Pb has been rather intractable to application of traditional models of collective motion. Until recently, most of the properties of the lowest-lying states could be understood only after numerical solution¹⁻³ of the full collective Hamiltonian. Recently a simpler picture, the interacting boson approximation (IBA) model of Arima and Iachello,⁴ has evolved. This model has its origin in the group symmetry properties of those identical nucleon (or nucleon hole) pairs in angular momentum states of $L=0$ or $L=2$ which are outside closed shells. The simplest geometrical models, the vibrational and rotational limits of the collective model, approximately correspond to possible subgroups [SU(5) and SU(3), respectively] for which the IBA Hamiltonian, having SU(6) group symmetry, might be symmetric. In the Os-Pt region the subgroup O(6) has been shown by Cizewski *et al.*⁵ to account for most of the energy and decay properties of all positive parity levels in ^{198}Pt below the pairing gap. Taking ^{198}Pt as the best example of O(6) symmetry the lighter mass even-even Os and Pt nuclei might be understood by breaking the O(6) symmetry with the introduction of a quadrupole-quadrupole interaction which introduces deformation to the nucleus.

The tests of the IBA model in its O(6) symmetry that have now been made in the Pt nuclei

include those by Cizewski *et al.*⁵ who have studied the gamma decay properties, and those by Deason *et al.*⁶ who have searched for low-lying $J^\pi = 0^+$ levels in $^{192,194,196}\text{Pt}$ using high resolution (p, l) reactions. Both studies located many new levels and found the O(6) limit predictions of branching ratios, level energies, and two-particle transfer strengths in good agreement with experiment.

Our present study of $^{194,196,198}\text{Pt}$ using the (p, p') reaction at 35 MeV also provides level energy and spin-parity information on these nuclei. Inelastic scattering is one of the few ways to study the most neutron-rich stable isotopes, such as ^{198}Pt . (Previously, only six levels in ^{198}Pt were known,⁷⁻⁹ and precise energies were known for only two of these.) The (p, p') reaction at 35 MeV is selective, can reach high spin ($J \approx 8$), and can be studied with high resolution (2-8 keV, using nuclear emulsion plates). Additionally, proton inelastic scattering angular distributions contain nuclear shape information. In this study we report on the population of approximately 45-50 levels in each nucleus to about 3 MeV excitation and the measurements of their energies. We use empirical shapes of angular distributions for excitations of levels with known J^π to make new J^π assignments. We then use relative matrix elements from the O(6) limit of the IBA model in a coupled channels approach in an attempt to describe the angular distributions for the low-lying levels. The parameters of the deformed optical model potential used in the coupled channels calculations are optimized to fit

these data, and the quadrupole and hexadecapole moments of the nuclear matter distribution for these Pt nuclei are deduced from this potential.

II. EXPERIMENTAL PROCEDURE

The inelastic scattering reactions were measured using 35 MeV protons from the Michigan State University isochronous cyclotron with scattered protons detected in the focal plane of the Enge split-pole spectrometer. Two detection techniques were employed: (1) a delay-line position-sensitive proportional counter¹⁰ with an energy resolution of 15 keV full width at half maximum (FWHM) (see Fig. 1), and (2) Kodak NTB-25 photographic emulsions (see Fig. 2) to obtain better resolution and precise values of level energies. The resolution was optimized by using a dispersion-matching technique.¹¹ The details for the beam monitoring and targets are given in Ref. 6. Angular distributions were extracted in the usual way from the counter data.

The experiments using emulsion plates were performed to calibrate the energy scales of the spectra from the counter experiments but also to determine precisely the level energies in

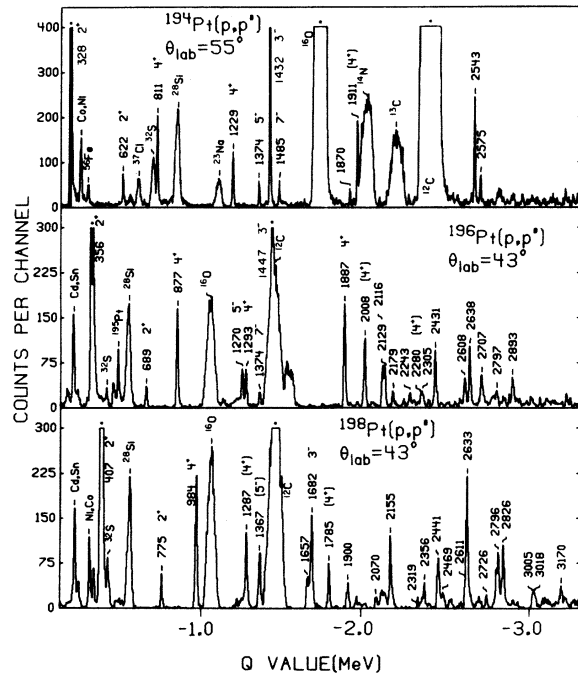


FIG. 1. Inelastic scattering proton spectra for the $^{194,196,198}\text{Pt}(p, p')$ reactions at 35 MeV. The data were obtained with nuclear emulsion plates. The elastic scattering peaks are not shown because they were too dense to scan. Peaks marked with an asterisk indicate that either the peak height has been cut off at the maximum value on the vertical axis or was unscannable.

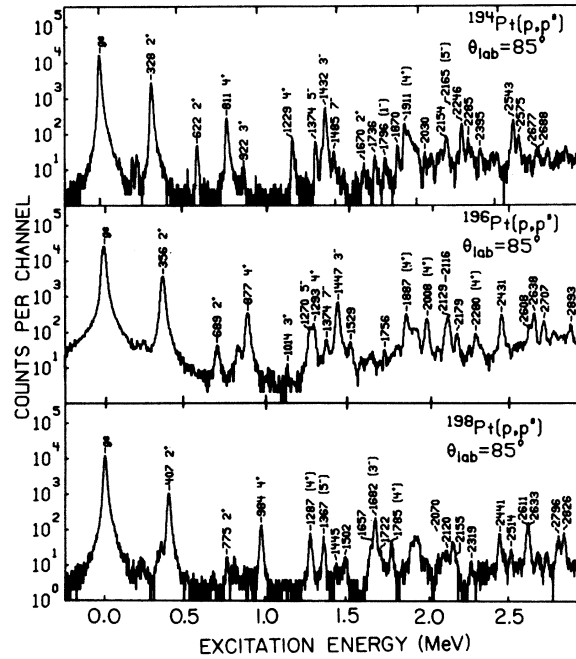


FIG. 2. Inelastic scattering proton spectra for the $^{194,196,198}\text{Pt}(p, p')$ reactions at 35 MeV. The data were obtained with a delay-line proportional counter.

^{198}Pt . For this latter purpose a thin target ($150 \mu\text{g}/\text{cm}^2$) of ^{206}Pb was used as well as the thin targets of $^{196,198}\text{Pt}$. The spectra from the $^{196,198}\text{Pt}$ and ^{206}Pb reactions were recorded on one photographic plate, at a fixed spectrograph angle. Only the vertical position of the plate in the focal plane was adjusted for each reaction, thus assuring an accurate relative calibration. The data were recorded at 43° and 75° to minimize the interference by the major contaminant reaction peaks, these being due to carbon, oxygen, and silicon. Peak areas and centroids were determined by using the computer code SCOPEFIT.¹² The different reaction kinematics and target thicknesses result in different energy losses so that the energies in ^{198}Pt relative to ^{196}Pt and ^{206}Pb cannot be directly used. Instead, the excitation energy per unit length is measured, this being the same for each spectrum. The energy calibrations of the ^{196}Pt and ^{206}Pb spectra were made by second order polynomial fits to known^{13,14} level energies, and also by using a kinematic routine (second order in momentum) to relate the momentum to the distance along the focal plane. Both methods agreed within the experimental uncertainties. The focal plane map was then used to energy calibrate the spectrum for the $^{198}\text{Pt}(p, p')$ reaction at 43° recorded on the plate. The uncertainties in level energies are typically 2 keV

below 2.5 MeV excitation energy and 0.1% in energy above 2.5 MeV.

III. EXPERIMENTAL RESULTS

A. General analysis

Approximately 45–50 levels were populated in each of the three reactions in the region below 3.0 MeV of excitation energy. In the case of $^{198}\text{Pt}(p, p')$, 38 of the 44 levels observed are reported for the first time. Only the energies of the first 2^+ and the second 0^+ states were accurately known before this study.^{7–9} The J^π assignment for the 0^+ state was tentative. Tables I–III summarize the excitation energies, cross sections ($\theta_{\text{lab}}=30^\circ$), and assignments of J^π from the $^{194,196,198}\text{Pt}(p, p')$ reactions. The results from previous studies of these nuclei are included and the results⁶ of the $^{196,198}\text{Pt}(p, t)$ reaction studies are shown for comparison.

An attempt was made to assign spin and parity to many of the states seen in each reaction, using

the distorted-wave Born approximation (DWBA) code DWUCK²⁹ and standard, collective model form factors. Except for the ground state, and the first 2^+ level for $\theta \approx 50^\circ$, the DWBA calculations provided very poor fits to the data. Thus, the spin assignments were based instead upon comparisons of angular distribution shapes to empirical shapes for states with well-known J^π , and from energy and spin systematics in the Pt nuclei.

B. Elastic scattering and $L=0$ transitions

The shape of the elastic angular distributions (Fig. 3) is virtually the same in each reaction. The most notable features at this energy are the “plateau” around 40° , a decrease in cross section of three orders of magnitude within the angular range studied, and three distinct minima between 50° and 100° .

In ^{194}Pt the two states at 1.547 and 1.892 MeV may be the well-known 0^+ states seen in several decay studies and in the (p, t) reaction study.⁶

TABLE I. States populated in the $^{194}\text{Pt}(p, p')$ reaction with comparisons to results from the $^{196}\text{Pt}(p, t)$ reaction and other studies.

E_x (MeV)	Present experiment $^{194}\text{Pt}(p, p')$		Previous results			
	J^π	σ (30°) ($\mu\text{b}/\text{sr}$)	E_x (MeV)	J^π	E_x^c (MeV)	J^π
0.0	0^+	5.00×10^5	0.0	0^+	0.0	0^+
0.328	2^+	5.03×10^3	0.328	2^+	0.3285	2^+
0.622 ^d	2^+	167	0.622	2^+	0.6221	2^+
0.811 ^d	4^+	328(40°)	0.811	4^+	0.8112	4^+
0.922(2)	(3^+)	26.6			0.9228	3^+
1.229 ^d	4^+	158	1.229	4^+	1.2295	4^+
			1.267	0^+	1.2671	0^+
1.374 ^d	5^-	77.5	1.374	($4^+, 5^-$)	1.3734	(5^-)
1.412	6^+	36.1	1.414(2)	6^+	1.4116	6^+
1.432 ^d	3^-	1.34×10^3	1.433	3^-	1.4325	3^-
			1.479(2)	0^+	1.4792	0^+
1.485 ^d	7^-	66.5	1.486(2)		1.4853	7^-
1.511(3)			1.512(3)		1.5119	2^+
1.529(2)						
1.547			1.547	0^+	1.5472	0^+
1.670	(2^+)	11.0(40°)	1.670		1.6706	2^+
1.736		28.3				
			1.778		1.7787	(1, 2, 3) ⁺
1.796		38.6			1.7974	1^-
1.815		14.8	1.815		1.817	(3^-)
1.870		123				
1.892			1.892		1.8936	0^+
1.911 ^d	(4^+)	457	1.911	(4^+)		
1.932	(5^-)	141	1.931		1.9302	(1, 2, 3) ⁺
1.948(3)		37.6	1.947		1.9485	
1.974						
1.981		22.1				
			1.990	($6^+, 7^-$)	1.9917	
			2.001		1.999	(8^-)

TABLE I. (Continued)

E_x (MeV)	Present experiment $^{194}\text{Pt}(p, p')$		Previous results			
	J^π	σ (30°) ($\mu\text{b}/\text{sr}$)	$^{196}\text{Pt}(p, t)^{194}\text{Pt}^a$ E_x (MeV)	J^π	Other results ^b E_x^c (MeV) J^π	
2.030		33.5	2.031		2.03	(2 ⁺)
			2.062		2.0638	
2.072		120				
2.104		37.0	2.105			
2.126	(4 ⁺)	105	2.125	(4 ⁺)	2.13	
			2.137			
2.154		145	2.155	(2 ⁺)	2.158	(1, 2) ⁺
2.165	(5 ⁻)	90.5				
2.912(4)		16.0	2.189			
			2.210			
2.222		41.0	2.224		2.22	
2.246		485	2.246	(4 ⁺)		
			2.277			
2.285		168	2.284		2.287	(1, 2) ⁺
			2.296	(7 ⁻ , 8 ⁺)	2.2961	1 ⁺
2.309		30.7			2.3098	
2.323(4)						
2.354		93.6	2.353	(4 ⁺)		
2.370(4)		29.1				
2.395		15.2			2.3975	
2.404		19.6(40°)				
2.418(4)		12.2				
2.536		90.8				
			2.532	(2 ⁺)		
2.543		609				
			2.566	(6 ⁺)	2.56	
2.575		154	2.580			
2.586(5)						
			2.595			
			2.638	(4 ⁺)		
2.677						
2.688(5)						
2.698			2.700	(6 ⁺)	2.7003	(11 ⁻)
			2.757			
			2.815			
			2.840			
			2.871			
			2.895			

^a Reference 6.^b References 7, 9, 15–23.^c The states above 2 MeV seen in this work and previous results are associated only because of similar energies.^d Used as calibration point with energy taken from Ref. 13. Uncertainties in excitation energy are approximately 1 keV below 1.9 MeV and 0.1% above 1.9 MeV, except as indicated.

These states are only weakly populated in the (p, p') reaction, and are not clearly resolved from nearby states in the wire counter data, so no angular distributions could be extracted. A level is seen at 1.826 MeV in ^{196}Pt which may be the known^{6,27} 0⁺ state at 1.823 MeV. An angular distribution was extracted for this level (see Fig. 3).

C. $L = 2$ transitions

Eight levels known to have $J^\pi = 2^+$ were populated in the three reactions, and in each case an angular distribution was obtained. The angular distributions for the first 2⁺ levels have less structure than do the second 2⁺ and higher-lying

TABLE II. States populated in the $^{196}\text{Pt}(p, p')$ reaction with comparisons to results from the $^{198}\text{Pt}(p, t)$ reaction and other studies.

E_x (MeV)	Present experiment $^{196}\text{Pt}(p, p')$		Previous results			
	J^π	σ (30°) ($\mu\text{b}/\text{sr}$)	E_x (MeV)	J^π	E_x^c (MeV)	J^π
0.0	0 ⁺	5.69×10^5	0.0	0 ⁺	0.0	0 ⁺
0.356	2 ⁺	4.55×10^3	0.356	2 ⁺	0.3557	2 ⁺
0.689 ^d	2 ⁺	48.7(40°)	0.689	2 ⁺	0.6889	2 ⁺
0.877 ^d	4 ⁺	258	0.877	4 ⁺	0.8770	4 ⁺
1.014(2)	3 ⁺	9.88(45°)			1.0152	3 ⁺
			1.135	0 ⁺	1.1352	0 ⁺
1.270 ^d	(5 ⁻)	180	1.271	5 ⁻	1.2705	(4, 5) ⁻
1.293 ^d	(4 ⁺)	269	1.293	(4 ⁺)		
			1.362		1.3617	(1 ⁺ , 2 ⁺)
1.374 ^d	7 ⁻	104	1.374	(6 ⁺ , 7 ⁻)	1.374	(6, 7) ⁻
			1.402	0 ⁺	1.4027	0 ⁺ , 1 ⁺ , 2 ⁺
1.447	3 ⁻	1.08×10^3	1.447	3 ⁻	1.4471	3 ⁻
1.529		77.0	1.527			
			1.537			
1.603(3)	2 ⁺	29.8	1.606	(2 ⁺)	1.6045	0 ⁺ , 1, 2 ⁺
1.679(3)		32.9	1.675(3)		1.677	2 ⁺
1.756(3)		37.7			1.7546	3, 4 [±] , 5 ⁻
			1.796			
1.826(3)		67.8	1.824	0 ⁺	1.8234	0 ⁺
			1.848	(2 ⁺)	1.8471	0 ⁺ , 1, 2
1.887	4 ⁺	536	1.884	(4 ⁺)	1.88	
1.964(3)			1.932			
			1.987			
2.008	(4 ⁺)	295	2.006			
2.055(3)			2.052			
			2.072			
			2.095			
2.116		179	2.114			
2.129		291	2.128		2.1289	1 ⁻ , 2 ⁺
			2.164		2.1627	0 ⁺ , 1, 2
2.179			2.174		2.1744	2 ⁺
			2.193		2.1908	0 ⁺ , 1, 2
			2.204		2.2044	2 ⁺
2.243		48.6			2.2455	(1, 2) ⁺
			2.264		2.2641	1, 2 ⁺
2.280	(4 ⁺)	65.0	2.277			
			2.296	(7 ⁻ , 8 ⁺)		
2.305		50.0			2.3092	(1, 2) ⁺
2.331(4)						
2.349					2.3453	1 ⁺ , 2 ⁺
2.360						
			2.370			
			2.386			
2.393					2.39	
			2.423			
2.431		541				
			2.440		2.442	0 ⁺ , 2 ⁺
			2.462		2.468	1 ⁺
2.469					2.4699	(1, 2) ⁺
2.505					2.5051	2 ⁺ (1 ⁻)
			2.521			
			2.533			
2.550			2.545		2.548	0 ⁺ , 2 ⁺
			2.557		2.57	
2.582						
2.608		230	2.609		2.60	
			2.627			

TABLE II. (Continued)

Present experiment $^{196}\text{Pt}(p, p')$			Previous results			
E_x (MeV)	J^π	σ (30°) ($\mu\text{b/sr}$)	$^{198}\text{Pt}(p, t)^{196}\text{Pt}^a$ E_x (MeV)	J^π	Other results ^b E_x^c (MeV)	
2.638		499	2.635		2.64	
			2.655			
			2.666		2.662	$0^+, 2^+$
			2.676		2.67	
2.707		298				
			2.759			
			2.766			
2.774(5)		90.5	2.779			
2.797		62.3(35°)				

^a Reference 6.

^b References 7, 9, 24–27.

^c The states above 2 MeV seen in this work and previous results are associated only because of similar energies.

^d Used as calibration point with energy taken from Ref. 13 along with (Ref. 28) the 0.803 10, 1.684 08, 2.200 23, and 2.647 90 MeV levels in ^{206}Pb . Uncertainties in excitation energy are approximately 1 keV below 1.8 MeV and 0.1% above 1.8 MeV, except as indicated.

2^+ levels; the angular distributions (Fig. 3) of the 0.328 MeV level in ^{194}Pt , the 0.356 MeV level in ^{196}Pt , and the 0.407 MeV level in ^{198}Pt display only mildly oscillatory shapes, while the 0.622 MeV level in ^{194}Pt and the 0.689 MeV level in ^{196}Pt exhibit more pronounced oscillations. However, the angular distribution for the 0.775 MeV level in ^{198}Pt has comparatively less structure. This may be the result of the decreasing deformation with increasing mass. Angular distributions for the first 2^+ states populated in the (p, p') reaction at 35 MeV on rare-earth nuclei,³⁰ where $\beta_2 \approx 0.23$, are more diffractive than those for the 2^+ states seen here. The assignment of a spin and parity of 2^+ for the 1.603 MeV level in ^{196}Pt supports the assignment made in the (p, t) study.⁶

D. $L=3$ transitions

States known to have $J^\pi = 3^-$ were very strongly excited at 1.432 MeV in ^{194}Pt and at 1.447 MeV in ^{196}Pt . The shape of the angular distributions for these states is very characteristic (see Fig. 4) and we assign the 1.682 MeV level in ^{198}Pt to have $J^\pi = 3^-$. A state has been observed⁷ at 1.722 MeV in ^{198}Pt and was assigned tentatively to have $J^\pi = 3^-$. We note, however, that the energies determined in Ref. 7 are systematically too high for the known levels populated in $^{194,196}\text{Pt}$, particularly for the higher lying states. Figure 4 includes the angular distribution for a 1.722 MeV level only weakly populated in the (p, p') reaction. The difference in strength between this level and

the known 3^- states in $^{194,196}\text{Pt}$ is a factor of 20. A definite assignment of J^π could not be made for the 1.722 MeV level.

Unnatural parity 3^+ states are seen in two of the reactions. Both states, at 0.922 MeV in ^{194}Pt and at 1.014 MeV in ^{196}Pt , are populated very weakly and complete angular distributions were not possible because of interference from impurity peaks. The partial angular distributions are included in Fig. 4. A possible $J^\pi = 3^+$ level is seen in ^{198}Pt at 1.246 MeV. This assignment is based only on systematics but has tentative support from a recent (n, n') study.³¹

E. $L=4$ transitions

At least three states with $J^\pi = 4^+$ were populated in each reaction. Each displays a similar, rather structureless angular distribution (Fig. 4). The major characteristics of these are a forward peak near 35° , a slight plateau at 60° , and a gradual decrease in strength towards backward angles. In ^{194}Pt four 4^+ states are identified. Two of these, at 0.811 and 1.229 MeV, were known from previous studies, while the level at 1.911 MeV was first seen in the (p, t) study.⁶ The state at 2.126 MeV is tentatively assigned to have $J^\pi = 4^+$, confirming the assignment made in the $^{198}\text{Pt}(p, t)$ study.⁶

Five states with $J^\pi = 4^+$ were observed in ^{196}Pt , including two which were previously known at 0.876 and 1.293 MeV. A third, at 1.887 MeV, may be the same state seen in the $^{198}\text{Pt}(p, t)^{196}\text{Pt}$ reaction⁶ (see Table II) although the energy is

TABLE III. States populated in the $^{198}\text{Pt}(p, p')$ reaction.

Present experiment $^{198}\text{Pt}(p, p')$			Previous results ^a	
E_x^b (MeV)	J^π	σ (30°) ($\mu\text{b}/\text{sr}$)	E_x^b (MeV)	J^π
0.0	0^+	4.92×10^5	0.0	0^+
0.407 ^c	2^+	3.24×10^3	0.4072	2^+
0.775	2^+	55.1(40°)	0.775	2^+
0.984	4^+	1.05×10^3	0.991	4^+
1.246(3)	(3^+)	21.9		
1.287	4^+	252	1.305	
1.367	(5^-)	142		
1.445(3)		56.6		
1.502(3)	(7^-)	82.8		
1.657		119		
1.682	3^-	845		
1.722(3)		25.5(40°)	1.722	(3^-)
1.785	(4^+)	150		
1.827(4)				
1.900		113		
1.949				
1.971(4)				
2.000				
2.070		46.6(40°)		
2.100		74.9		
2.120		57.9		
2.155		137		
2.178		52.7		
2.319				
2.339				
2.356				
2.387				
2.441		369		
2.469		49.9		
2.514		108		
2.573		36.3	2.53	
2.611		762		
2.633				
2.666		96.5		
2.726		62.3		
2.782				
2.796		325		
2.826		385		
2.884		38.4		
2.910		38.0		
3.005				
3.018				
3.170(5)				
3.197(5)				

^a References 7-9.^b Uncertainties in the excitation energies are approximately 2 keV below 2.5 MeV and 0.1% above 2.5 MeV, except where indicated.^c Used as calibration point along with the 0.80310, 6.68408, 2.20023, and 2.64790 MeV levels from ^{206}Pb (Ref. 28).

3 keV higher for the state seen in the proton scattering (the energy uncertainties are about 2 keV for each reaction). Two additional states have been tentatively assigned to have $J^\pi = 4^+$, at 2.008 and 2.280 MeV. These states may have been observed in the (p, t) study.⁶

Three states in ^{198}Pt have been assigned to have $J^\pi = 4^+$. The lowest lying one is at 0.984 MeV [0.991 MeV in an (α, α') study⁷]. The third 4^+ state is at 1.785 MeV. Thus, three 4^+ states are seen at about 2 MeV excitation in each of $^{192,194,196,198}\text{Pt}$. The nature of these states is unknown, but their strengths in inelastic proton scattering may indicate a considerable hexa-decapole component. This will be discussed below.

F. Transitions with $L \geq 5$

Five $L=5$ transitions have been assigned on the basis of the empirical shape of the angular distribution for the probable 5^- state at 1.374 MeV in ^{194}Pt (Fig. 5). The 5^- state seen in ^{198}Pt at 1.270 MeV was previously assigned²⁶ to have $J^\pi = (4, 5)^-$ but the (p, t) study⁶ preferred $J^\pi = (5^-)$. Assignments of $J^\pi = (5^-)$ were made in ^{194}Pt for levels at 1.932 and 2.165 MeV.

Only one angular distribution (Fig. 5) was obtained for a level known to have $J^\pi = 6^+$, the 1.412 MeV level in ^{194}Pt . The uncertainties are quite large at most angles because of its weak population and its proximity to the strongly populated 3^- level at 1.432 MeV. No attempt was made to extract an angular distribution for the 6^+ level in ^{198}Pt because the strongly populated 3^- level is only 17 keV away.

Angular distributions were obtained for the 1.485 MeV level in ^{194}Pt and 1.374 MeV level in ^{198}Pt (Fig. 5). The level at 1.485 MeV in ^{194}Pt was previously known to have $J^\pi = 7^-$ from in-beam γ -decay studies,¹⁹ thus affording an empirical shape for comparison in the $^{196,198}\text{Pt}(p, p')$ reactions. The level at 1.374 MeV in ^{198}Pt had been previously assigned as $(6^+, 7^-)$, but its angular distribution suggests $J^\pi = 7^-$. An assignment of $J^\pi = (6^+, 7^-)$ has also been made for the level at 1.502 MeV in ^{198}Pt . A level at 1.722 MeV in ^{198}Pt could not be given an assignment because of its weak population.

Figure 5 includes twelve seemingly unique angular distributions: three from ^{194}Pt , four from ^{196}Pt , and five from ^{198}Pt , all with essentially the same features, the most prominent of which is a strong maximum at 50° on an otherwise smoothly decreasing cross section. The levels are at relatively high excitation energies, from 2.1 to 2.8 MeV. The transitions to them are some of the strongest in each reaction. Unfortunately,

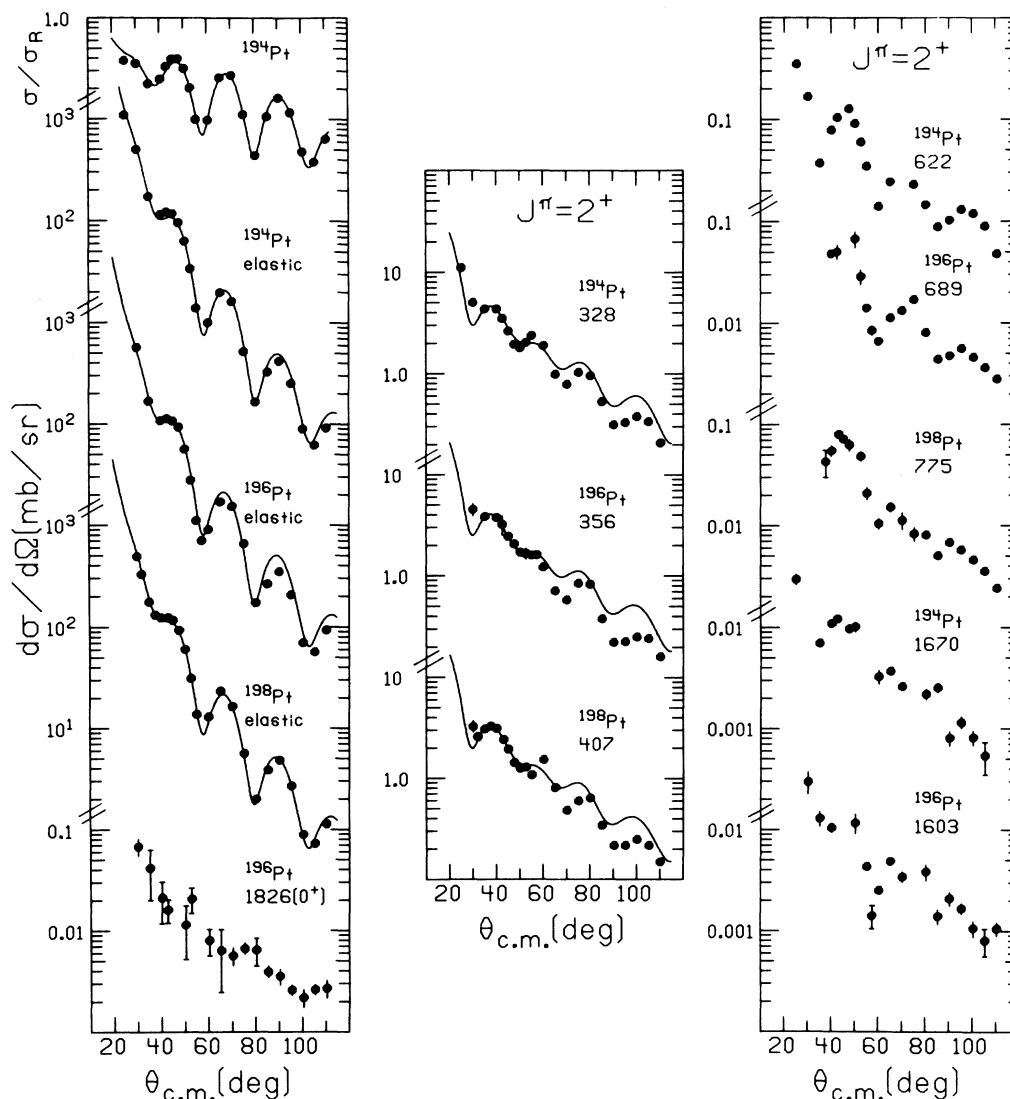


FIG. 3. Elastic scattering and $L=0, 2$ angular distributions from the $^{194,196,198}\text{Pt}(p, p')$ reactions. The curves are the results of DWBA calculations using a collective model form factor. Energies are given in keV. The uppermost curve in the left panel is representative of the angular distributions of the ratio of elastic-to-Rutherford scattering differential cross sections; here, the curve is for ^{194}Pt .

there are no known levels in any of the reactions with a similar shape, so no spin information can be obtained. However, the strength of these transitions and their high excitation energy (approximately 1 MeV above the pairing gap at about 1.4 MeV) may indicate these states are composed of highly correlated, particle-hole configurations. Further investigation is needed, though, before a definite characterization of these states can be made.

Several additional angular distributions are shown in Fig. 6. No spin assignments were made

for these transitions because of large uncertainties in the angular distribution data.

IV. COUPLED CHANNEL ANALYSIS OF THE INELASTIC SCATTERING DATA

Attempts to describe the inelastic scattering data with the DWBA were not very successful. Only the shape of the first 2^+ angular distribution for the three reactions could be reasonably reproduced (see Fig. 3). Since there is only one form factor for a given L transfer in the collec-

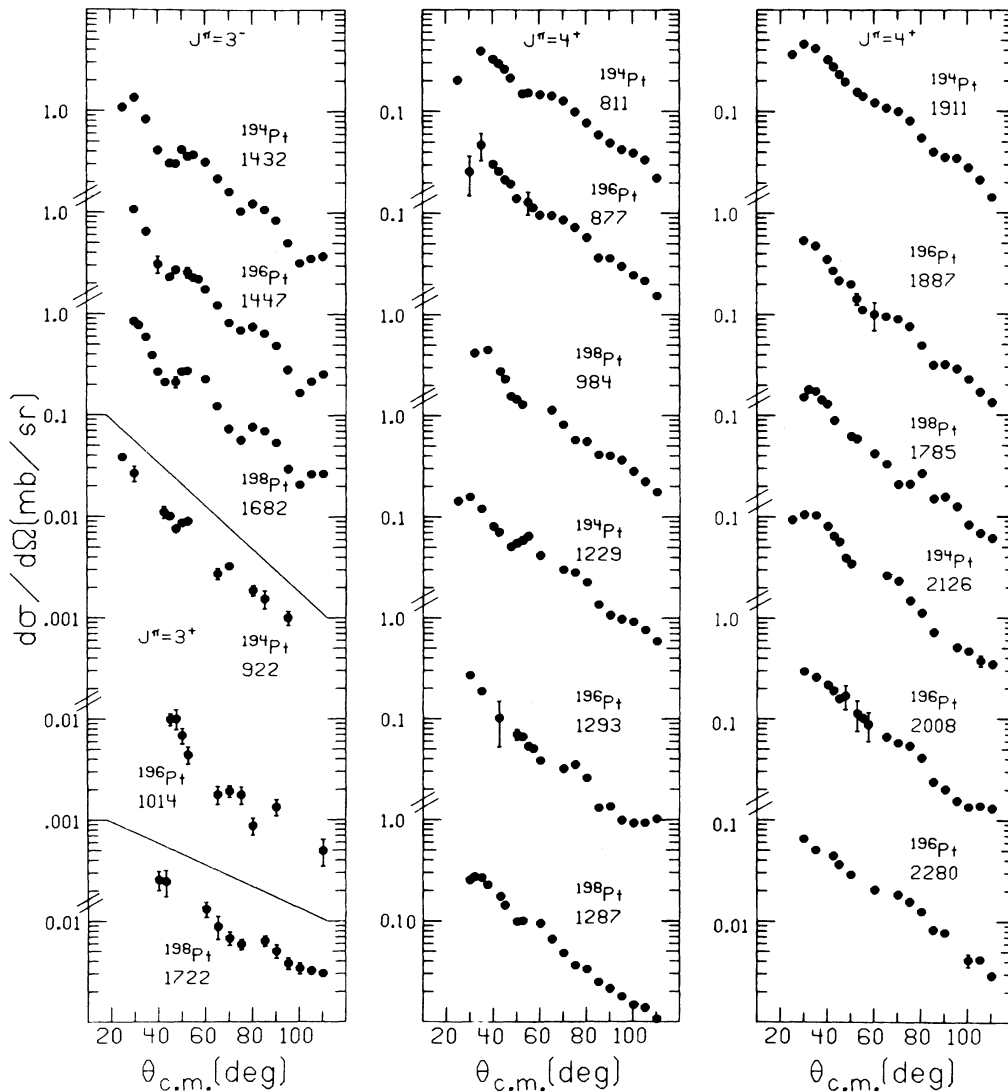


FIG. 4. $L = 3, 4$ angular distributions from the $^{194,196,198}\text{Pt}(p, p')$ reactions. Energies are given in keV.

tive model approach, there is no way to account for the dramatically different 2^{+} angular distribution. Hence, the more complete coupled channels approach is necessary.

The procedures used in this study for the coupled channel analysis are similar to those employed for the analysis of proton scattering from well-deformed nuclei.³⁰ Briefly, an iterative searching procedure determines the best set of optical model parameters for reproducing the elastic scattering data. Next, the deformation parameters β_{λ}^N are determined for the ground band by a similar, searching procedure, where a "best fit" (minimum values of χ^2) is obtained for the inelastic data as well as for the elastic data.

These calculations were performed using the coupled channels code ECIS.³²

Additionally, the effects of several other features of the data and theory were investigated, such as spin-orbit effects, the coupling of the quasi- γ band, and the use of matrix elements derived from the IBA model⁴ to describe the coupling between the nuclear states. Finally, we have used a multipole moment technique to compare the results of this analysis to the results of other studies of nuclear deformations of $^{194,196,198}\text{Pt}$.

A. The optical model analysis

The starting point of the coupled channels calculation is the determination of the best set of

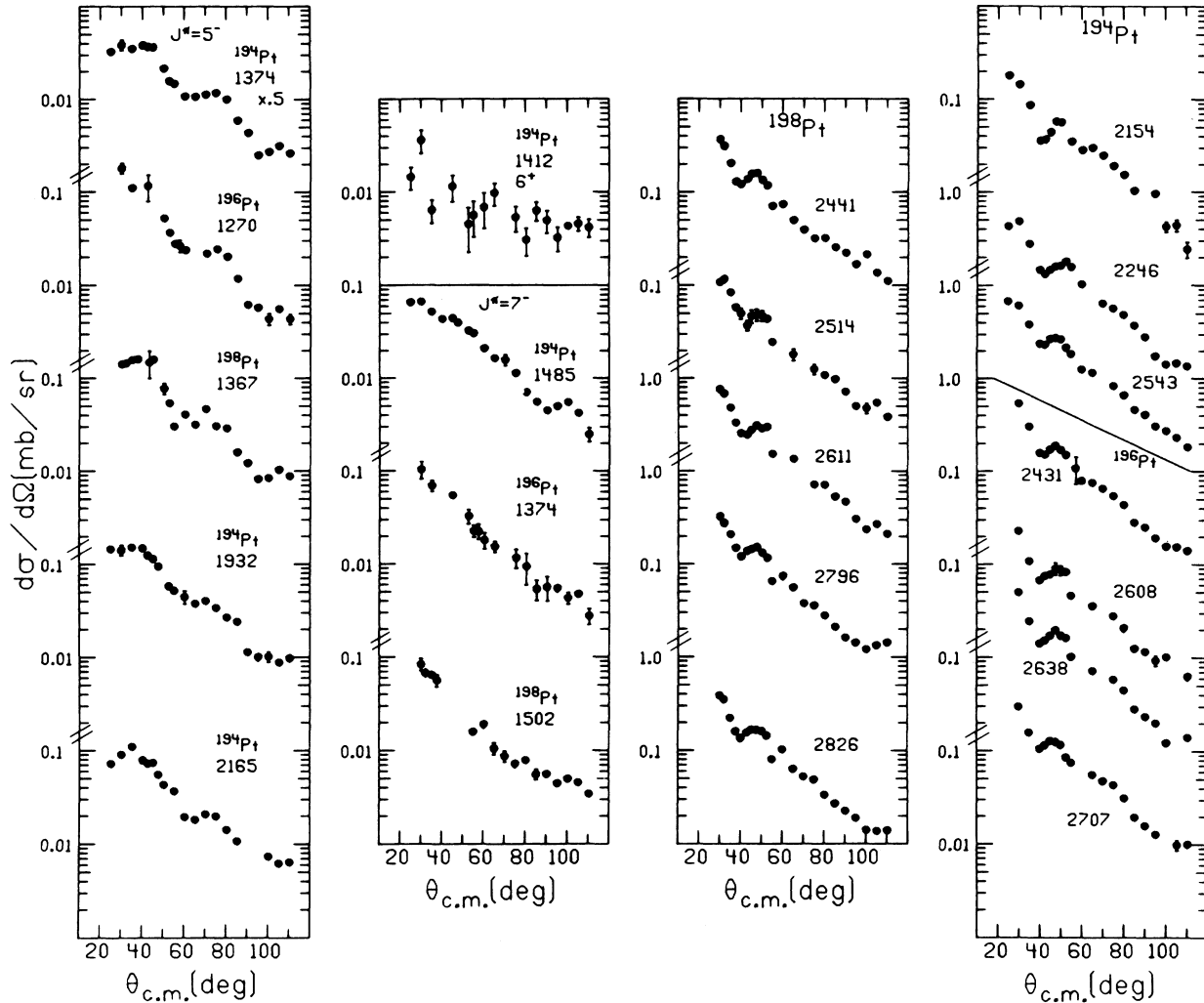


FIG. 5. $L \geq 5$ angular distributions from the $^{194,196,198}\text{Pt}(p, p')$ reactions. In the third and fourth panels are angular distributions with unique shapes unlike those for levels with known J^π . Energies are given in keV.

parameters for the optical potential which will reproduce the experimental elastic scattering. We employ a standard deformed optical model potential (DOMP). The shape of the potential is assumed to have the deformed Woods-Saxon form with the deformation parameterized via the expansion

$$R = R_0 \left[1 + \sum_{\lambda} \beta_{\lambda} Y_{\lambda 0}(\theta) \right], \quad R_0 = r_0 A^{1/3}.$$

The Coulomb part of the potential is derived from a deformed uniform charge distribution with a sharp cutoff. There are eleven optical model parameters that could be included in a search: V , W , W_D , V_{SO} , r_R , r_I , r_{SO} , r_C , a_R , a_I , and a_{SO} plus several deformation parameters, β_{λ}^N and β_{λ}^C . We limited the number of varied parameters

to V , W_D , V_{SO} , a_R , a_I , and β_{λ}^N (β_{λ} , hereafter) to simplify the searching process. The starting values of all parameters in the searches and the values of W , r_R , r_I , r_{SO} , and a_{SO} were taken from the work of Becchetti and Greenlees.³³ However, the parameters held constant throughout the searches were not chosen arbitrarily. The radius parameters were not included in the searches because they enter the coupling potential as products with their respective deformation parameters. The Coulomb parameters r_C , β_2^C , and β_4^C , were taken from Ref. 7. The imaginary well depth was held constant primarily for simplification.

The optimum standard optical model parameters were determined by use of the automatic searching features in ECIS to minimize the chi-squared

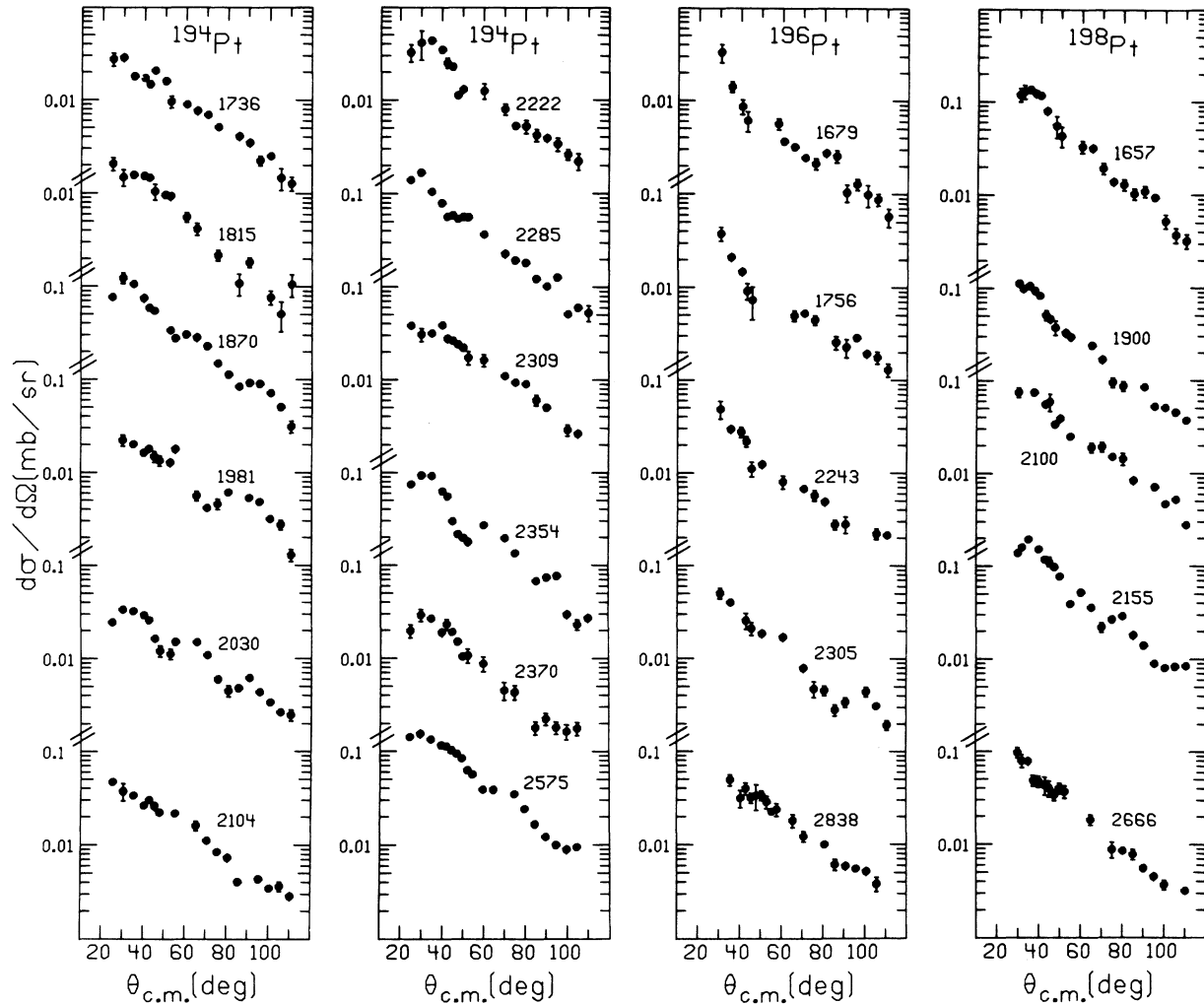


FIG. 6. Angular distributions from $^{194,196,198}\text{Pt}(p, p')$ reactions with unknown L transfer. Energies are given in keV.

value for the ground state, χ_0^{2+} . These calculations included couplings between the 0^+ , 2^+ , and 4^+ levels. The parameter search was conducted by simultaneously varying either the three potential depths (V, W_D, V_{SO}) or the diffuseness parameters (a_R, a_I). The sequence of searches typically involved two iterations of a search on the well depths followed by a search on the diffuseness parameters, one search on the deformation parameter β_2 while minimizing χ_0^{2+} , then two more iterations on (V, W_D, V_{SO}) and (a_R, a_I). The starting β_λ values were deduced from values in Ref. 7. The Coulomb and nuclear matrix elements are assumed to have the same relative values (discussed below) although each set is normalized to the $0^+ \rightarrow 2^+$ and $0^+ \rightarrow 4^+$ matrix elements which are calculated in ECIS from the DOMP. All the calcu-

lations were performed using 25 partial waves, an integration step size of 0.33 fm, and a matching radius of 20 fm. The multipole expansion included couplings of $\lambda=2$ and $\lambda=4$ terms to $L=8$. For simplicity, the nuclear deformations were equal for the real and the imaginary portions of the potential.

The search results are given in Table IV for calculations employing a deformed full Thomas form³⁴ for the spin-orbit term (L^*S), and for calculations without a spin orbit ($L^*S=0$), as discussed below. The changes in the parameters from Becchetti-Greenlees parameters³³ when $L^*S \neq 0$ are relatively small except for values of the real diffuseness a_R and the imaginary surface term W_D . These decrease by about 7% and 12%, respectively.

TABLE IV. Optical model parameters used in the coupled channels calculations.

Nuclide	V^a (MeV)	a_R (fm)	W_D (MeV)	a_I (fm)	V_{SO} (MeV)	χ^2/N (ground state)
^{194}Pt						
$L * S:$						
$\kappa = 0.0375$ keV	53.40	0.712	4.70	0.663	6.497	7.0
$\kappa = 0.5375$ keV	53.12	0.723	4.82	0.658	6.466	8.6
$L * S = 0:$						
$\kappa = 0.0375$ keV	51.84	0.659	8.13	0.594	0.0	14.3
$\kappa = 0.5375$ keV	51.64	0.656	7.99	0.604	0.0	15.1
^{196}Pt						
$L * S$	51.78	0.786	5.46	0.666	6.551	17.1
$L * S = 0$	50.79	0.734	7.86	0.644	0.0	29.9
^{198}Pt						
$L * S$	53.35	0.709	4.72	0.667	6.475	5.5
$L * S = 0$	52.53	0.624	7.60	0.611	0.0	10.2

^a The β_{χ}^C and r_C values are taken from Ref. 7. All radii were held constant, $r_R = 1.17$ fm, $r_I = 1.32$ fm, $r_{SO} = 1.01$ fm, and $r_C = 1.2$ fm. Also, the spin-orbit diffuseness a_{SO} was held constant (1.01 fm), and W retained the Becchetti-Greenlees (Ref. 33) value of 5.1 MeV for ^{194}Pt and 5.0 MeV for $^{196}, ^{198}\text{Pt}$.

B. The IBA matrix elements

Since relatively little is known about the matrix elements which connect the low-lying states of the Pt nuclides (except³⁵ in the case of ^{194}Pt), one must use a nuclear structure model which makes predictions of matrix elements. This allows a test of the predictive qualities of the nuclear structure model beyond comparisons of energy levels and transition rate ratios. With the recent success of the O(6) limit of the IBA in the Pt-Os region for energy levels, $E2$ branching ratios,⁵ and (p, t) strengths,⁶ the coupled channel analysis of the (p, p') reaction should provide a natural framework for further testing the $E2$ and $E4$ matrix elements. We note that our data on ^{194}Pt could not be well described³⁶ using simple collective models.

The matrix elements used in the analysis were obtained from the computer code PHINT³⁷ which diagonalizes the IBA Hamiltonian. We use a "perturbed" O(6) Hamiltonian. In the O(6) limit the eigenvalues are given by

$$E(N, \sigma, \tau, \nu_{\Delta}, J) = \frac{A}{4} (N - \sigma)(N + \sigma + 4) + B\tau(\tau + 3) + CJ(J + 1),$$

where A , B , and C are constants, N is the number of bosons, and σ , τ , ν_{Δ} , and J are quantum num-

bers (see Ref. 5 for a detailed discussion). Deviations from this limit can be introduced by including a term for the quadrupole-quadrupole interaction between bosons,⁵ whose strength is given by κ . It should be noted that the introduction of this term is still within the context of the IBA model and only requires⁴ a more complete solution of the full IBA Hamiltonian.

Small values of κ primarily affect the magnitude of transitions which are not allowed in the strict O(6) limit because of the $\Delta\tau = 1$ selection rule. The matrix elements most affected are $M_{02'}$, M_{23} , $M_{24'}$, $M_{34'}$, and $M_{2'4'}$, where

$$M_{j_k} = - \langle k || M(E2) || j \rangle.$$

Also, the "reorientation" matrix elements M_{JJ} are altered because of the increased mixing of the wave functions. Our experiment using protons is not sensitive to these. The parameter input to PHINT is taken from Ref. 5 and is listed in Table V. The values used in the ^{198}Pt calculations were obtained by extrapolating prescribed⁵ relationships: A is held constant, B and C are varied linearly with mass, and κ is varied logarithmically with mass. Casten and Cizewski⁵ point out that the transition rates are sensitive only to the ratio κ/B , which specifies the location of the nucleus relative to the O(6) and rotor limits; the values of κ or B individually are not

TABLE V. IBA parameters used in the perturbed O(6) calculations. A , B , and C are the coefficients of the pairing, O(5), and O(3) components, respectively, of the O(6) Hamiltonian, and κ is the strength of the quadrupole-quadrupole interaction. N is the total number of bosons for each nucleus.

Nucleus	N	A (keV)	B (keV)	C (keV)	κ (keV)	κ/B	
^{194}Pt	Set 1	7	186	42.0	17.5	0.0375	0.0009
	Set 2	7	186	42.0	17.5	0.5375	0.0128
^{196}Pt	6	186	43.0	19.0	0.025	0.0006	
^{198}Pt	5	186	43.5	20.5	0.016	0.004	

critical. The calculated matrix elements are shown in Table VI. Two sets are given for ^{194}Pt , one from $\kappa=0.0375$ keV,⁵ and one from $\kappa=0.5375$ keV.

C. The extraction of deformation parameters

Once the set of optical model parameters giving the optimal fit to the ground state angular distribution was obtained, the values of the deformation parameters were extracted using the optical

model parameters of Table IV and the IBA matrix elements of Table VI. The values of β_2 and β_4 were varied simultaneously, to minimize χ^2 , defined as the sum of the chi-squared values for the ground state, 2^+ , and 4^+ state angular distributions. An angular distribution was obtained for the 6^+ state in ^{194}Pt but its χ^2 was not included in those calculations because couplings to the 8^+ state were not included due to computing limitations when $L*S \neq 0$. The results of this analysis of the angular distributions for the ground band states excited in $^{194,196,198}\text{Pt}$ are shown in Fig. 7 as the solid line fits. The deformation parameters are given in Table VII. The quality of the fits is quite good even though the relative values of the matrix elements were not varied.

Additional calculations were performed for each nucleus to investigate the effects of the spin-orbit interaction. Searches were performed on the optical model parameters with $L*S=0$. There was a significant increase in W_D which decreased the depths of the minima (increased absorption) compared to the deep minima which result if the Becchetti-Greenlees parameters³³ are used with $L*S=0$. Such an effect is understandable in that the spin-orbit interaction is surface peaked and

TABLE VI. Relative matrix elements for $^{194,196,198}\text{Pt}$ calculated using the O(6) symmetry in the IBA model.

r	s	^{194}Pt $\kappa=0.0375$ keV		^{194}Pt $\kappa=0.5375$ keV		^{196}Pt $\kappa=0.025$ keV		^{198}Pt $\kappa=0.016$ keV	
		$-M_{rs}(E2)$	$M_{rs}(E4)$	$-M_{rs}(E2)$	$M_{rs}(E4)$	$-M_{rs}(E2)$	$M_{rs}(E4)$	$-M_{rs}(E2)$	$M_{rs}(E4)$
0	2_1	-1.0		-1.0		-1.0		1.0	
0	2_2	0.004 6		0.062 7		0.002 42		-0.001 23	
0	4_1		1.0		1.0		1.0		1.0
0	4_2		-0.002 67		0.036 9		-0.001 31		-0.000 6
2_1	2_1	-0.014 2	1.380	-0.196	1.376	-0.007 3	1.436	-0.003 5	1.521
2_1	2_2	-1.156	-0.003 70	-1.142	-0.050 8	-1.144	-0.002 0	-1.127	-0.001 1
2_1	4_1	1.551	-0.015 2	1.552	-0.209	-1.535	0.008 1	-1.512	0.004 15
2_1	3	-0.006 1	0.559	-0.083 8	0.557	0.003 14	-0.544		
2_1	4_2	0.001 1	0.818	-0.015 5	-0.802	0.000 6	0.797	-0.000 36	-0.763
2_1	6		-1.426		-1.425		-1.388		-1.329
2_2	2_2	0.014 2	0.656	0.196	0.659	0.007 3	0.694	0.003 53	0.751
2_2	4_1	0.002 9	-1.721	-0.039 7	1.269	0.001 6	1.818	0.000 85	1.970
2_2	3	-1.186	-0.003 59	-1.186	-0.049 4	1.155	0.001 7		
2_2	4_2	-1.152	-0.015 2	1.155	0.210	-1.121	-0.007 95	1.073	0.003 98
4_1	4_1	-0.012 7	0.087 8	-0.175	0.883	-0.006 3	0.927	-0.002 95	1.004
4_1	3	0.750	-0.003 99	0.074 8	0.005 51	0.730	-0.002 3		
4_1	4_2	1.098	-0.005 72	-1.090	0.078 7	-1.069	0.003 0	1.024	-0.001 56
4_1	6	-1.913	0.013 0	-1.914	0.180	1.862	0.006 9	1.783	-0.003 46
4_1	8		-1.622						
3	3		-1.767		-1.765		1.901		
3	4_2	0.007 42	-0.748	0.103	0.744	-0.006 4	0.804		
3	6		-1.452		1.446		1.564		
4_2	4_2	0.006 94	1.525	0.094 9	1.512	0.003 6	1.641	0.001 79	1.820
6	6	-0.010 1	0.965	-0.141	0.969	-0.004 8	1.038	-0.002 04	1.152
6	8	2.120	-0.011						
8	8	-0.007 52	1.133						

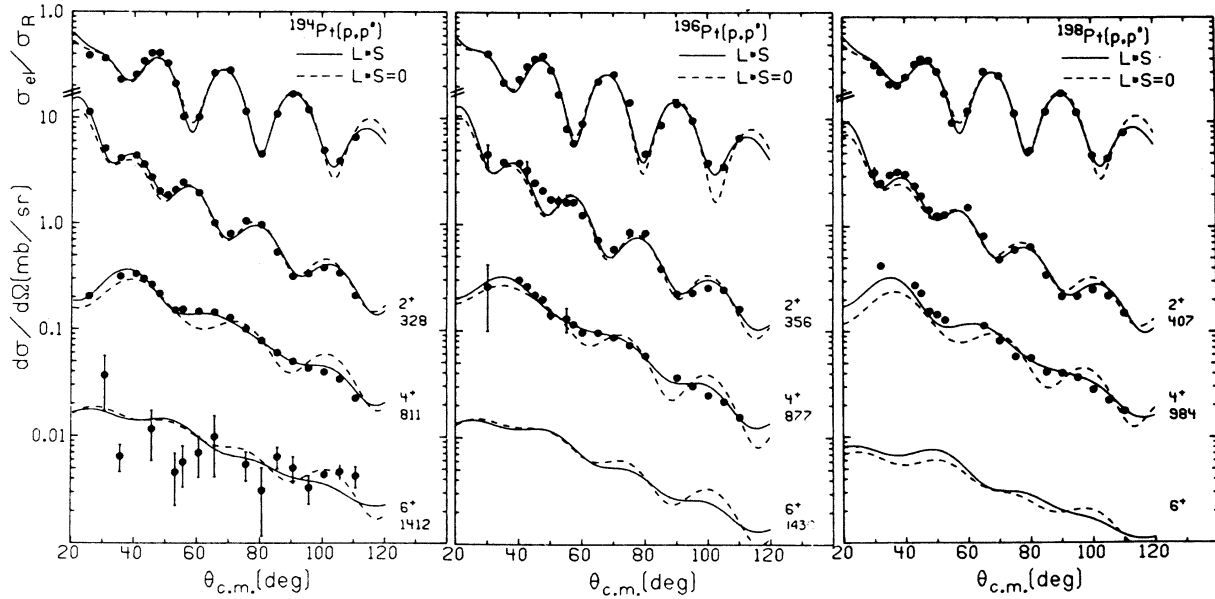


FIG. 7. Data and coupled channels calculations for $^{194,196,198}\text{Pt}(p, p')$ with ($L*S$) and without ($L*S=0$) the spin-orbit interaction. The calculations used the matrix elements of Table V, and DOMP parameters from Tables IV and VII.

turning this interaction off causes the surface imaginary term to absorb some of the effects. Table VII also shows the results of searches when $L*S=0$. Comparisons of the spin-orbit versus no-spin-orbit calculations are also shown in

Fig. 7. The most obvious difference is the more pronounced oscillations in the $L*S=0$ calculations, especially for the 4^+ calculations. (The value of χ^2 for each level is nearly twice as large as values for the calculations using the spin-orbit

TABLE VII. Deformation parameters and potential moments obtained from $0^+-2^+-4^+-6^+$ coupled channel calculations for $^{194,196,198}\text{Pt}$. Values from calculations with ($L*S$) and without ($L*S=0$) a spin-orbit interaction are included.

Nucleus	β_2	β_4	q_2 (b)	q_4 (b ²)
^{194}Pt				
$\kappa = 0.0375^a$				
$L*S$	-0.154(2)	-0.0455(10)	-1.32(2)	-0.156(7)
$L*S=0$	-0.168(3)	-0.0566(17)	-1.40(2)	-0.184(12)
$\kappa = 0.5375$				
$L*S$	-0.151(2)	-0.0453(10)	-1.30(2)	-0.160(6)
$L*S=0$	-0.164(3)	-0.0550(20)	-1.37(3)	-0.181(12)
^{196}Pt				
$\kappa = 0.025$				
$L*S$	-0.142(3)	-0.0485(13)	-1.25(3)	-0.202(11)
$L*S=0$	-0.152(5)	-0.0573(21)	-1.31(5)	-0.226(16)
^{198}Pt				
$\kappa = 0.016$				
$L*S$	-0.119(2)	-0.0422(20)	-1.05(2)	-0.177(7)
$L*S=0$	-0.128(4)	-0.0479(30)	-1.09(4)	-0.181(18)

^a The unit for κ is keV.

interaction.) However, although the values of β_2 and β_4 when $L \cdot S = 0$ are significantly different, the moments (as discussed below) in each case are comparable. We used calculations without spin orbit to investigate the effects of a variety of couplings not possible on our computer with the inclusion of spin-orbit terms.

D. Sensitivity of coupled channel calculations to higher order couplings and selected matrix elements

1. The sign of β_4

Earlier theoretical calculations (e.g., Ref. 38) and experiments^{7,39} have indicated a negative value of β_4 for the Pt nuclides. A series of calculations were performed to investigate the sensitivity of the (p, p') data to the sign of β_4 . Figure 8 compares the result of a $0^+ - 2^+ - 4^+ - 6^+$ calculation for ^{194}Pt with a positive, negative, and zero value for β_4 . This calculation included the spin-orbit interaction. Using a negative β_4 value, the overall slope and the fit to the first maximum are in agreement with the data. The oscillations for a positive value of β_4 (dashed line fit in Fig. 8) are almost completely out of phase with those for $\beta_4 < 0$, and the cross section is overestimated at backward angles. Also, the value of $\chi^2_{2^+}$ increases by a factor of 2. The calculation with $\beta_4 = 0$ clearly fails to reproduce the data. The necessity of including a β_4 component is also discussed in Sec. IVD 5, concerning the second 4^+ level. The present results support earlier findings^{7,39} of a negative value of β_4 for the Pt isotopes. Although there might be evidence⁴⁰ in the rare-earth region for small values of β_6 this was not investigated.

2. The effect of the "quasi- γ " band couplings

In order to test further the O(6) IBA matrix elements, calculations were performed including the lowest states of the "quasi-gamma" band, whose bandhead is the second 2^+ state. Three previous inelastic scattering studies of the Pt nuclei have also studied members of this band. These states are the 2^{+1} , 3^+ , and 4^{+1} states in $^{194,196}\text{Pt}$ and the 2^{+2} and 4^{+2} states in ^{198}Pt . The calculations included both β_2 and β_4 deformations, the IBA matrix elements in Table VI, and $L \cdot S \neq 0$. The IBA $0^+ - 4^{+1}$ matrix element relative to that for $0^+ - 4^+$ is extremely small and a larger value was necessary to reproduce the data.

The results of these calculations for ^{194}Pt are shown in Fig. 9 for two different sets of matrix elements. One set was calculated using PHINT,³⁴ the parameters of Ref. 5, and $\kappa = 0.0375$ keV. The second set was calculated using $\kappa = 0.5375$ keV. This larger value of κ gives a value for $B(E2; 2^{+2} - 0^+)/B(E2; 2^{+1} - 2^+)$ closer to the experimental one than when $\kappa = 0.0375$ keV. The calculations fit better the angular distribution for the 2^{+2} state, but at the expense of the already poorly fit 3^+ and 4^{+1} state data. The value of $\kappa = 0.5375$ keV is almost twenty times larger than that used in Ref. 5, but it is not unrealistically large. In fact, values in the Os region⁵ are an order of magnitude still larger than those in the Pt region.

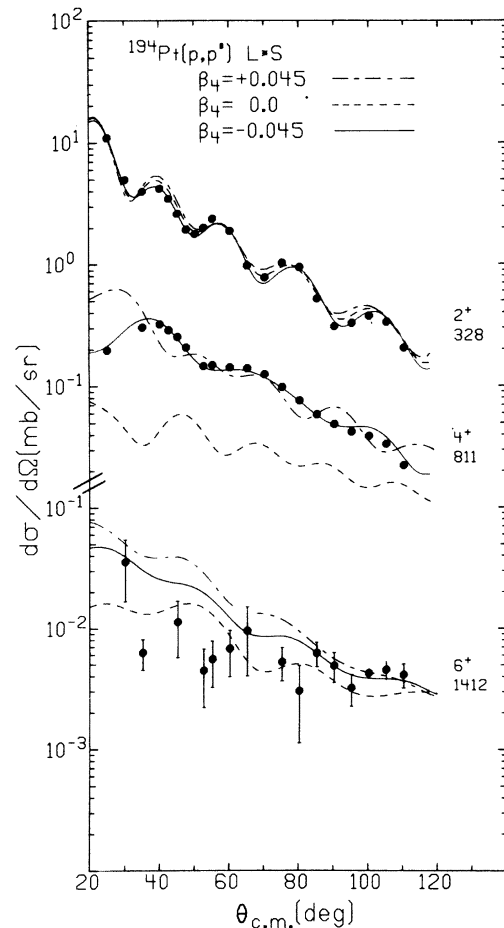


FIG. 8. Data and coupled channels calculations using $0^+ - 2^+ - 4^+ - 6^+$ level couplings for $^{194}\text{Pt}(p, p')$ with positive, negative, and zero values for β_4 . These calculations used in the IBA matrix elements of Table V and the DOMP parameters of Tables IV and VII. The spin-orbit interaction was included and $\beta_2 = -0.172$.

$2^{+2} - 0^+)/B(E2; 2^{+1} - 2^+)$ closer to the experimental one than when $\kappa = 0.0375$ keV. The calculations fit better the angular distribution for the 2^{+2} state, but at the expense of the already poorly fit 3^+ and 4^{+1} state data. The value of $\kappa = 0.5375$ keV is almost twenty times larger than that used in Ref. 5, but it is not unrealistically large. In fact, values in the Os region⁵ are an order of magnitude still larger than those in the Pt region.

3. The effect of the 2^{+2} state on the β_λ values

To test the influence the 2^{+2} state may have on extracting the deformation parameters, a search was made on β_2 and β_4 simultaneously using $0^+ - 2^+ - 4^+ - 2^{+2}$ level couplings and the IBA matrix elements with $\kappa = 0.5375$ keV. The χ^2 values were minimized for each level. Similarly, a search

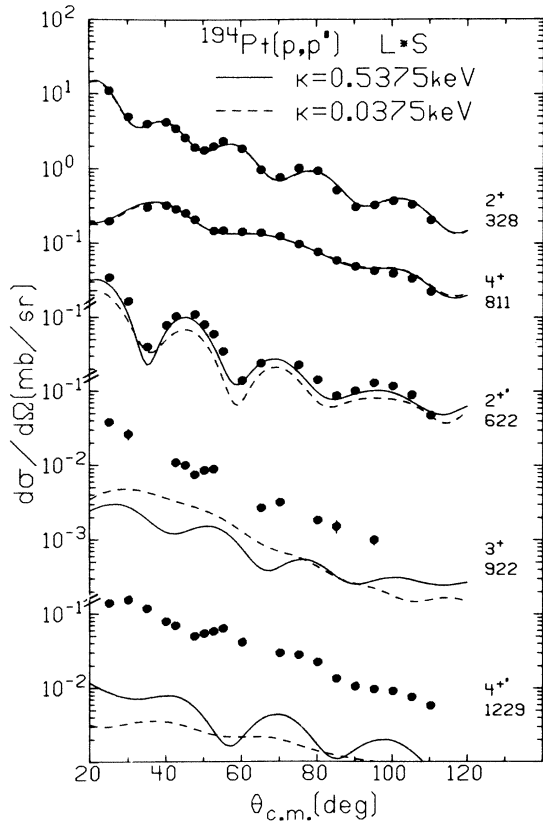


FIG. 9. Data and coupled-channels calculations for the $^{194}\text{Pt}(p, p')$ reaction using the spin-orbit interaction and two sets (Table V) of IBA matrix elements, $\kappa = 0.0375$ keV (solid curve) and $\kappa = 0.5375$ keV (dashed curve). The DOMP parameters are given in Tables IV and VII.

was made using $0^+ - 2^+ - 4^+ - 6^+$ level coupling. Both calculations used the same initial values for β_2 and β_4 , and in each calculation, $\chi_T^2 (= \chi_0^2 + \chi_2^2 + \chi_4^2)$ minimized for the same final values within statistical uncertainties. However, the better fit was obtained from the $0^+ - 2^+ - 4^+ - 6^+$ calculation. The relatively weak coupling of the 2^{+1} state, indeed the weak coupling of the quasi- γ band, indicates that calculations involving only ground band couplings are sufficient for determining the deformation parameters.

4. The sign of P_3

One of the principal motivations for the earlier inelastic scattering studies on the Pt nuclides^{7,39,41} was to determine the sign of $P_3 = M_{02} M_{02} M_{22}$. P_3 describes the interference between the one-step and two-step paths that populate the second 2^+ state. Baker *et al.*^{7,39} found that a negative value for P_3 was needed to fit their (α, α') reaction data on $^{192,194}\text{Pt}$. This was unexpected since both the

asymmetric rotor³ and pairing-plus-quadrupole^{42,43} models predict $P_3 > 0$. Baker *et al.*^{7,39,41} also concluded that large values of M_{04} and M_{04}' are needed to explain the shape and strength of the 4^{+1} angular distributions. However, it was shown⁴¹ that by including the symmetric hexadecapole components (Y_{40}) in the asymmetric rotor shape (Davydov model³), the fit to the first 4^+ level was improved. A negative value of P_3 was also then consistent with the predictions of this "extended" asymmetric rotor model.

We investigated the sensitivity of the (p, p') data to the sign of the interference term. Figure 10 shows the results of calculation for ^{194}Pt , performed with the matrix elements in Table VI coupling the 0^+ , 2^+ , 4^+ , and 2^{+1} levels, with $L \cdot S \neq 0$. The sign of P_3 was changed by changing the sign of M_{02}' . The data are fit much better when $P_3 < 0$, in agreement with the earlier study.⁷ This is also true for similar IBA calculations for ^{196}Pt . The perturbed O(6) IBA calculations correctly predict the sign of P_3 in both sets of matrix elements calculated for ^{194}Pt , and for ^{196}Pt . For $^{198}\text{Pt}(p, p')$ the calculations with $P_3 < 0$ provide slightly better fits to the data, even though the calculations predict $P_3 > 0$. However, for ^{198}Pt , M_{02}' is a small, negative number, -0.0012 . This difference in sign from the $^{194,196}\text{Pt}$ O(6) predictions

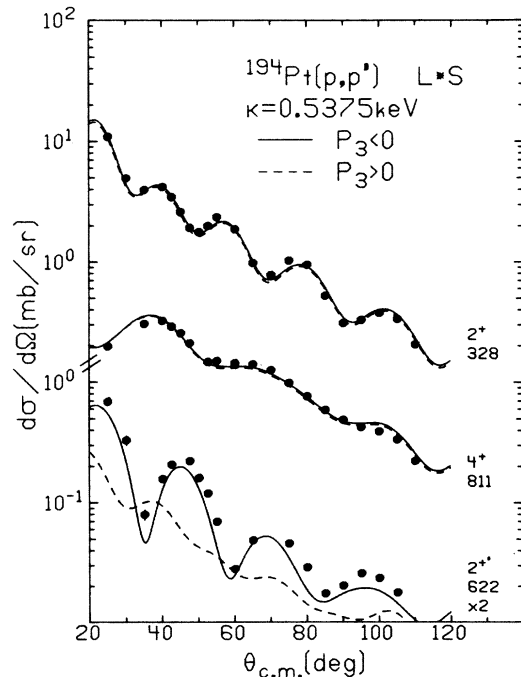


FIG. 10. Data and coupled channels calculations for the $^{194}\text{Pt}(p, p')$ reaction with positive (dashed curve) and negative (solid curve) values for the interference term P_3 . Note that the data and theory for the 2^{+1} state have been multiplied by 2. Here, $\beta_2 = -0.151$ and $\beta_4 = -0.0453$.

is partially understandable. In the strict $O(6)$ limit, $M_{02'} = 0$ because of the $\Delta\tau$ selection rule. With the addition of a small perturbation, via the parameter κ , the selection rule is broken and small values of $M_{02'}$ are obtained. The value of P_3 remains negative because the sign of M_{02} changes as well. The cause of this sign change is not understood. To draw definite conclusions about the role of P_3 for ^{198}Pt it will be necessary to secure a better value for κ from γ -ray branching ratios because of the influence of P_3 on small matrix elements.

5. The $M_{04'}$ matrix element

The coupled channel calculations using $O(6)$ matrix elements fail to describe the 4^{+} angular distributions in $^{194,196,198}\text{Pt}$. A similar effect was seen in the (α, α') study by Baker *et al.*³⁹ The major cause of this failure is the small predicted hexadecapole matrix element between the ground state and second 4^{+} level. To improve the fit a search was performed on the $0-4^{+}$ matrix elements, using the IBA values for the other matrix elements as given in Table VI. The search was performed without the spin-orbit term so that a $0^{+}-2^{+}-4^{+}-2^{+}-3^{+}-4^{+}$ level space could be used (except for ^{198}Pt where no 3^{+} couplings were included). The shapes of the 4^{+} angular distribution with and without the spin-orbit couplings are similar. The results of these calculations are

shown as the solid curves in Fig. 11 for $^{194,196,198}\text{Pt}$. The best fit for the 4^{+} angular distribution is obtained in the ^{198}Pt case, with the rather structureless shape except for a maximum at 35° . The other three calculations show considerably more diffraction for this angular distribution. Table VIII summarizes the $M_{04'}$ and $B(E4)$ values as well as these values from the $^{192}\text{Pt}(\alpha, \alpha')$ reaction.³⁹ Baker *et al.*³⁹ obtained a better fit to their data with a positive value for $M_{04'}$; our values are negative for ^{194}Pt and positive for $^{196,198}\text{Pt}$. However, these matrix elements depend on the two-step and three-step excitation routes to the 4^{+} level, leading to an uncertainty in value as is shown in Table VIII for ^{192}Pt . The best fit values obtained in this study are thus significant only for the values of M_{02} , $M_{22'}$, $M_{24'}$, and $M_{02'}$.

E. Comparison of charge and nuclear potential moments

Mackintosh,⁴⁴ using a theorem by Satchler,⁴⁵ has shown that the multipole moments of the real part of the DOMP are proportional to the moments of the nuclear matter density, if the DOMP for protons is derivable from a reformulated optical model potential. This assumes that the nucleon-nucleon interaction is independent of density, and that the proton and neutron distributions have equal deformations. The multipole moment

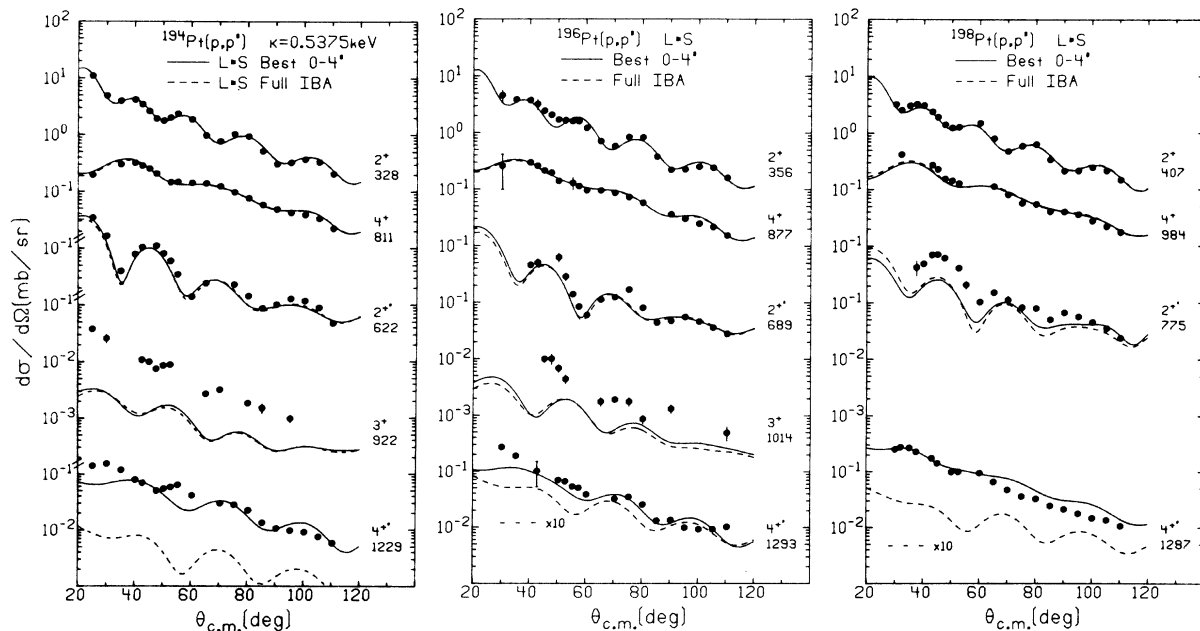


FIG. 11. Data and coupled channels calculations for the $^{194,196,198}\text{Pt}(p,p')$ reactions. For ^{194}Pt , $\kappa = 0.5375$ keV. The dashed curves represent calculations with the IBA matrix elements of Table VI while the solid curves represent the calculations when $M_{04'}$ is increased. The calculations for ^{198}Pt did not include couplings to the 3^+ state.

TABLE VIII. Summary of $0^+ \rightarrow 4^{++}$ matrix elements and $B(E4)$ values for $^{192-198}\text{Pt}$.

Nucleus	M_{04} (eb^2)	$B(E4; 0^+ \rightarrow 4^{++})$ (e^2b^4)	$B(E4; 0^+ \rightarrow 4^+)$ (e^2b^4)
$^{192}\text{Pt}^a$	+0.34	0.12	0.041
	-0.20	0.040	0.041
^{194}Pt			
$\kappa = 0.0375$	-0.12	0.014	0.024
$\kappa = 0.5375$	-0.11	0.012	0.026
^{196}Pt	+0.14	0.020	0.041
^{198}Pt	+0.21	0.043	0.031

^a Reference 39.

method is a more fundamental approach to compare results from Coulombic and hadronic scattering experiments. The β_λ , or the "deformation lengths" $\beta_\lambda R$, where R is the potential radius, are reaction dependent quantities. Inelastic nucleon scattering cross sections depend on the product $\beta_\lambda R$, whereas Coulomb excitation cross sections are proportional to the squares of the $E\lambda$ matrix elements, which have a first order $\beta_\lambda R^\lambda$ dependence. The product $\beta_\lambda R$ may also be correlated with other optical model parameters.

Following the suggestion by Mackintosh, the multipole moments q_2 and q_4 were calculated from the real part of the DOMP using the relation

$$q_\lambda = \frac{K \int V(\vec{r}) r^\lambda Y_{\lambda 0}(\theta) d\vec{r}}{\int V(\vec{r}) d\vec{r}}.$$

The DOMP parameters are those given in Tables IV and VII. When K is chosen to be equal to Z , the proton number, the comparison can be made with results from electromagnetic excitation studies. The moments from our study are given in Table IX along with moments from Coulomb excitation^{33,41,46} and those calculated from the DOMP and Coulomb potentials used in an (α, α') reaction study.⁷ The Coulomb deformation parameters obtained in Refs. 40 and 7 are those for a uniform charge distribution with a sharp cutoff, for asymmetrically and symmetrically deformed shapes, respectively. The potential moments in the present study and in Ref. 7 are for a deformed Fermi distribution.

A comparison of the (p, p') results with those from the previous experiments indicates the q_2 potential moments from proton scattering are in much better agreement with the charge moments from Coulomb excitation than are the potential moments of Baker *et al.*,⁷ determined by using the (α, α') reaction. The moments from (p, p') are in general systematically larger in magnitude

than moments of the charge potentials from Coulomb excitation and (α, α') but this is perhaps statistically significant only for q_2 in ^{194}Pt and q_4 in ^{196}Pt . In each nucleus the charge component

TABLE IX. $E2$ and $E4$ moments in $^{194,196,198}\text{Pt}$.

Nuclide	Method	q_2^a (b) or (eb)	q_4^a (b^2) or (eb^2)
^{194}Pt	(p, p') at 35 MeV ^b	-1.32(2)	-0.156(7)
	Coulomb excitation ^c	-1.273(6)	
	($^{12}\text{C}, ^{12}\text{C}$) ^d	-1.269	-0.1486
	(α, α') ^e P	-1.52	-0.30
	C	-1.31	-0.12
^{196}Pt	(p, p') at 35 MeV ^b	-1.25(3)	-0.202(11)
	Coulomb excitation ^f	-1.22(5)	
	(α, α') ^e P	-1.38	-0.24
	C	-1.17	-0.097
^{198}Pt	(p, p') at 35 MeV ^b	-1.05(2)	-0.177(7)
	Coulomb excitation ^f	-1.00(3)	
	(α, α') ^e P	-1.12	-0.32
	C	-1.08	-0.14

^a The units for the charge component moments are b^λ , $\lambda=2$ or 4 . The units for the electromagnetic moments are eb^λ .

^b These moments were obtained using the DOMP parameters, including the spin-orbit interaction, contained in Tables IV and VII.

^c Reference 35.

^d Reference 41.

^e Reference 7. The first value reported is the potential moment (P) and the second value is the charge distribution moment (C).

^f Reference 46.

of the proton potential moment is in better agreement with the charge moment from Refs. 7 and 41 rather than the potential moment,⁷ except perhaps in ¹⁹⁸Pt. Possible reasons for the deviation between moments from proton scattering and moments determined by electromagnetic means have been discussed by King *et al.*³⁰ The discrepancy between α -scattering potential moments and Coulomb excitation values has been discussed by Mackintosh⁴⁴ and is thought to be an indication that phenomenological α -scattering potentials are not currently derivable from reformulated optical model potentials.

V. LEVEL ENERGIES IN ¹⁹⁸Pt AND SYSTEMATICS OF THE Pt ISOTOPES

It is convenient to describe the energy level systematics in the stable Pt nuclei by starting with the O(6) limit and then breaking the symmetry by increasing the strength of the boson quadrupole-quadrupole interaction. Casten and Cizewski⁵ have interpreted energy level and branching ratio systematics in the Pt-Os region in this manner. At the time little was known about ¹⁹⁸Pt. Here we apply the perturbed O(6) limit, with the suitable⁵ value of κ , to ¹⁹⁸Pt. In Fig. 12 we show the levels in ^{192,194,196,198}Pt. The striking experimental feature in ¹⁹⁸Pt is the grouping of the 2^{+} , 0^{+} , and 4^{+} levels around a centroid energy slightly larger than twice the energy of the 2^{+} level. This is reminiscent of the SU(5) (vibrational) limit predictions. The calculated values do show the proper level sequence but quite different spacings for the 2^{+} and 3^{+} states. It is difficult to understand this behavior because nuclei at the beginning of shells should have SU(5)

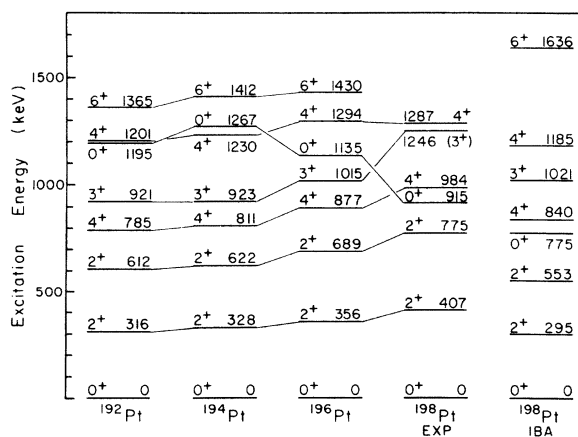


FIG. 12. Systematics of experimentally determined level energies for positive parity states in ^{192,194,196,198}Pt. The data for ¹⁹⁸Pt are compared to calculations using the perturbed O(6) limit of the IBA model with $\kappa = 0.016$ keV.

symmetry and the nuclei at the end of shells should have O(6) symmetry. We do note that our calculations are extrapolations of the trends for the lighter Pt isotopes and that the parameters for each nucleus are not optimized. We also neglect proton-neutron boson interactions, a procedure which affects⁴⁷ the calculated level energies considerably more than γ -ray matrix elements.

VI. SUMMARY

Many level energies in ^{194,196,198}Pt were measured using the (p, p') reaction at 35 MeV. In ¹⁹⁸Pt, 38 of the 44 levels below about 3.2 MeV are reported for the first time. Angular distributions were measured, and comparisons to empirical shapes of angular distributions for levels with known J^π values allowed several new spin assignments. The angular distributions of the ground band levels, with $J^\pi = 0^+, 2^+, 4^+$ (and for ¹⁹⁴Pt, 6^+), and the low-lying $J^\pi = 2^{+'}, 3^+, 4^{+'}$ quasi- γ band levels were analyzed within a coupled channels framework of an oblate rotor with a negative β_4 shape component but using relative matrix elements from the O(6) limit of the IBA model of Arima and Iachello. The angular distributions for the ground band states and the $2^{+'}$ state angular distribution are well described using this approach. The $4^{+'}$ state angular distribution can be satisfactorily fit only by allowing a direct $L=4$ excitation of this state. The sensitivity of the calculations to several effects was noted: the sign of the $L=2$ matrix element product which connects the $J^\pi = 0^+, 2^+$, and $2^{+'}$ levels; the quadrupole strength parameter κ in the IBA model; and the effect of the quasi- γ band on the extraction of the moments. The extracted moments are systematically more negative but are in better agreement with values from Coulomb excitation than are the moments derived from the DOMP parameters used in (α, α') studies.

Note added in proof. We have become aware of two very recent studies of ^{194,196,198}Pt. Using the (t, p) reaction, Cizewski *et al.* [Phys. Rev. C (to be published)] have studied ^{196,198}Pt, as well as ²⁰⁰Pt. Using heavy-ion-induced Coulomb excitation, Bolotin *et al.* [Phys. Rev. C (to be published)] have also studied ^{196,198}Pt. The energies of those levels excited in their studies as well as ours are in good agreement with our results. They provide also supplementary level energy and structure information on ^{196,198}Pt.

ACKNOWLEDGMENTS

We wish to express our gratitude to Dr. R. F. Casten, Dr. J. A. Cizewski, Dr. S. W. Yates,

and Dr. J. P. Delaroche for their interest in our study and for helpful discussions with us. We are indebted to Dr. J. Raynal for his code ECIS and for communications pertaining to its use. This

material is based upon work supported by the National Science Foundation under Grant No. Phys 78-22696.

- *Present address: E. I. DuPont Corporation, Savannah River Plant, Aiken, S.C. 29801.
- †Present address: Bell Laboratories, Murray Hill, N.J. 07974.
- ‡Present address: Physics Division, Argonne National Laboratory, Argonne, Ill. 60439.
- ¹G. Gneuss and W. Greiner, Nucl. Phys. A171, 449 (1971).
- ²T. Kishimoto and T. Tamura, Nucl. Phys. A192, 246 (1972); A270, 317 (1976).
- ³Krishna Kumar and Michel Baranger, Nucl. Phys. 122, 273 (1968).
- ⁴A. Arima and F. Iachello, Ann. Phys. (N.Y.) 99, 253 (1976); 111, 201 (1978); 123, 468 (1979); Phys. Rev. Lett. 40, 385 (1978).
- ⁵J. A. Cizewski, R. F. Casten, G. J. Smith, M. L. Stelts, W. R. Kane, H. G. Börner, and W. F. Davidson, Phys. Rev. Lett. 40, 167 (1978); R. F. Casten and J. A. Cizewski, Nucl. Phys. A309, 477 (1978).
- ⁶P. T. Deason, C. H. King, T. L. Khoo, J. A. Nolen, Jr., and F. M. Bernthal, Phys. Rev. C 20, 927 (1979).
- ⁷F. T. Baker, Alan Scott, T. H. Kruse, W. Hartwig, E. Ventura, and W. Savin, Nucl. Phys. A266, 337 (1976).
- ⁸E. J. Bruton, J. A. Cameron, A. W. Gibb, D. B. Kenyon, and L. Keszthelyi, Nucl. Phys. A152, 495 (1970).
- ⁹Paresh Mukherjee, Nucl. Phys. 64, 65 (1965).
- ¹⁰R. G. Mar'ham and R. G. H. Robertson, Nucl. Instrum. Methods 129, 131 (1975).
- ¹¹H. G. Blosser, G. M. Crawley, R. Deforest, E. Kashy, and B. H. Wildenthal, Nucl. Instrum. Methods 91, 61 (1971).
- ¹²H. David (unpublished).
- ¹³M. R. Schmorak, Nucl. Data Sheets 7, 395 (1972).
- ¹⁴R. L. Auble, Nucl. Data Sheets 7, 95 (1972).
- ¹⁵O. Bergman and G. Bäckström, Nucl. Phys. 55, 529 (1964).
- ¹⁶A. W. Sunyar, G. Scharff-Goldhaber, and M. McKeown, Phys. Rev. Lett. 21, 237 (1968); 21, 506 (1968).
- ¹⁷G. D. Benson, A. V. Ramayya, R. G. Albridge, and G. D. O'Kelley, Nucl. Phys. A150, 311 (1970).
- ¹⁸J. V. Maher, J. R. Erskine, A. M. Friedman, R. H. Siemssen, and J. P. Schiffer, Phys. Rev. C 5, 1380 (1972).
- ¹⁹S. W. Yates, J. C. Cunnane, R. Hochel, and P. J. Daly, Nucl. Phys. A222, 301 (1974).
- ²⁰W. E. Cleveland and E. F. Zganjar, Z. Phys. A 279, 195 (1976).
- ²¹I. Y. Lee, D. Cline, P. A. Butler, R. M. Diamond, J. O. Newton, R. S. Simon, and F. S. Stephens, Phys. Rev. Lett. 39, 684 (1977).
- ²²S. A. Hjorth, A. Johnson, Th. Lindblad, L. Funke, P. Kemnitz, and G. Winter, Nucl. Phys. A262, 328 (1976).
- ²³R. M. Ronningen, R. B. Piercey, A. V. Ramayya, J. H. Hamilton, S. Raman, P. H. Stelson, and W. K. Dagenhart, Phys. Rev. C 16, 571 (1977).
- ²⁴L. V. Groshev, A. M. Demidov, and A. S. Rakhimov, Yad. Fiz. 7, 937 (1968)[Sov. J. Nucl. Phys. 7, 563 (1968)].
- ²⁵J. F. W. Jansen, H. Pauw, and C. J. Toeset, Nucl. Phys. A115, 321 (1968).
- ²⁶C. Samour, H. E. Jackson, J. Julien, A. Bloch, C. Lopata, and J. Morgenstern, Nucl. Phys. A121, 65 (1968).
- ²⁷J. A. Cizewski, R. F. Casten, G. J. Smith, M. R. Macphail, M. L. Stelts, W. R. Kane, H. G. Börner, and W. F. Davidson, Nucl. Phys. A323, 349 (1979).
- ²⁸M. P. Webb, Nucl. Data Sheets 7, 95 (1972).
- ²⁹P. D. Kunz (unpublished).
- ³⁰C. H. King, J. E. Finck, G. M. Crawley, J. A. Nolen, Jr., and R. M. Ronningen, Phys. Rev. C 20, 2084 (1979).
- ³¹S. W. Yates (private communication); S. W. Yates, A. Khan, M. C. Mirzaa, and M. T. McEllistrem (unpublished).
- ³²J. Raynal (unpublished).
- ³³F. D. Becchetti and G. W. Greenlees, Phys. Rev. 182, 1190 (1969).
- ³⁴J. Raynal, *The Structure of Nuclei* (IAEA, Vienna, 1972).
- ³⁵C. Baktash, J. X. Saladin, J. J. O'Brien, and J. G. Alessi, Phys. Rev. C 18, 131 (1978).
- ³⁶J. P. Delaroche (private communication).
- ³⁷O. Scholten (unpublished).
- ³⁸U. Götz, H. C. Pauli, K. Alder, and K. Junker, Nucl. Phys. A192, 1 (1972).
- ³⁹F. T. Baker, Alan Scott, R. M. Ronningen, T. H. Kruse, R. Suchanek, and W. Savin, Phys. Rev. C 17, 1559 (1978).
- ⁴⁰D. L. Hendrie, N. K. Glendenning, B. H. Harvey, O. N. Jarvis, H. H. Duhm, J. Saudinos, and J. Mahoney, Phys. Lett. 26B, 127 (1968).
- ⁴¹F. Todd Baker, Alan Scott, T. P. Cleary, J. L. C. Ford, E. E. Gross, and D. C. Hensley, Nucl. Phys. A321, 222 (1979).
- ⁴²A. S. Davydov and G. F. Fillippov, Nucl. Phys. 8, 327 (1958).
- ⁴³K. Kumar, Phys. Lett. 29B, 25 (1969).
- ⁴⁴R. S. Mackintosh, Nucl. Phys. A266, 379 (1976).
- ⁴⁵G. R. Satchler, J. Math. Phys. 13, 1118 (1972).
- ⁴⁶J. E. Glenn, R. J. Pryor, and J. X. Saladin, Phys. Rev. 188, 1905 (1969).
- ⁴⁷R. F. Casten (private communication).